IEEE Access
Multidisciplinary | Rapid Review | Open Access Journal

Received January 21, 2021, accepted January 29, 2021, date of publication February 3, 2021, date of current version February 9, 2021.

Digital Object Identifier 10.1109/ACCESS.2021.3056666

Decimetre Level Range Resolution for Beidou B3I Signal-Based Passive SAR Imaging—Proof-of-Concept Experimental Demonstrations

YU ZHENG[1], ZHUXIAN ZHANG[2], PENG WU[1,2], AND PEIDONG ZHU[1,3], (Senior Member, IEEE)

[1]College of Electronic Communication and Electrical Engineering, Changsha University, Changsha 410022, China
[2]College of Electronic Science, National University of Defense Technology, Changsha 410073, China
[3]College of Computer Science and Technology, National University of Defense Technology, Changsha 410073, China

Corresponding author: Yu Zheng (y_zheng170@sina.com)

This work was supported in part by the National Natural Science Foundation of China under Project 42001297, in part by the research grants from the Education Department of Hunan Province, China, under Project 18C0758, and in part by the research grant from Changsha University under Project SF1903.

ABSTRACT The construction of the Beidou B3 satellite system, a new-generation global navigation satellite system, has been completed worldwide, however the respective implementation studies remain in the start-up stage. Accordingly, studies of passive Beidou B3I signal-based synthetic aperture radar (Beidou B3I-SAR) are very meaningful in terms of promoting the rapid development of the Beidou technique. This paper proposes methods for Beidou B3I SAR imaging of decimetre level range resolution. To separate aliased reflected B3I signals at range domain, we presented cascaded secondary order differentiation operator (Diff2) and cascaded Teager-Kaiser (TK) operator, applied them to the regions where exists range compressed pulses, respectively. Thereafter to eliminate the obvious side-lobes which brought by the proposed operators and with the values less than zero, zero thresholding scheme is employed. To obtain the final range compressed signals with decimetre range resolution, phase recovery component is performed to the respective zero thresholded pulses. To validate the proposed methods, both proof of concept simulation and the experiment with field Beidou B3I signal raw data are carried out for comparison. The results show that indeed main-lobe width of range compressed pulse can reach the level 0.4 m. This reveals that decimetre level range resolution can be achieved for Beidou B3I-SAR on the basis of proposed methods, in contrast to the current best result of meters level in passive GNSS-based SAR related studies. Meanwhile, in a comparison of the proposed methods on the basis of cascaded Diff2 operator and cascaded TK operator, the later is outer-performed, since the respective brought interference level in background region is less.

INDEX TERMS Beidou B3I signal, synthetic aperture radar, reflected signal, range resolution.

I. INTRODUCTION

Global Navigation Satellite System (GNSS) is a satellite communication system that transmits wireless radio navigation signal and provides position service at a global level [1], [2]. In this field, Beidou system has aroused number of research attentions recent years. Till 2020, Beidou system, including the new generation Beidou system - B3 system, has completed the global constructions [3]. However, the related implementation based research is still at a start-up stage. To promote the development of Beidou technique, studies of remote sensing imaging based on the Beidou B3I signal, which is known as passive Beidou B3I-based synthetic aperture radar (Beidou B3I SAR), are very important. In comparison to traditional types of active radar, Beidou B3I SAR is a type of passive radar [4], [5]; it does not require a constructed radar transmission module and enables a more flexible installation at a low cost under many surveillance scenarios [6]. Like other GNSS signals, Beidou B3I signals cover the globe and are not subject to transmission failure, thus Beidou B3I SAR can work under all day all weather circumstance, compared to other type passive radars such as

The associate editor coordinating the review of this manuscript and approving it for publication was Zhongyi Guo.

DVB-T signal based radar [7]. In terms of Beidou B3I SAR imaging, resolution is a vital issue to be addressed.

For resolution issue with respect to passive SAR using other types of GNSS signals i.e. GPS C/A signal, GLONASS signal, Galileo signal and Beidou B1 signal, there already has several related works [8]–[24]. Among them, for bi-static GNSS-SAR system, range resolution (the main-lobe width of range compressed pulse) is determined by signal bandwidth and bi-static angle [8], [20], [21], while azimuth resolution is determined by dwell time and the trace for forming synthetic aperture imaging [12], [21]. This paper specifically considers range resolution. In most studies, bi-static angle is considered as fixed, then the wider bandwidth, the higher range resolution. For instance, in the works [8]–[17], [19], Beidou-2 signal, GLONASS signal and single band Galileo E5 signal were employed for passive SAR imaging, the respective range resolutions with fixed optimal bi-static angle were achieved at the levels 75 m, 50 m and 15 m. Since GNSS signals are not originally designed for surveillance purpose, compared to other environmental surveillance tools, range resolution for passive GNSS based SAR is relatively lower than that of other environmental surveillance tools. To improve range resolution, in 2015, the researchers [20] utilized full bandwidth Galileo E5 signal (i.e. joint Galileo E5a/b) to obtain the range resolution to 3 m level. However the scheme still does not address the problem that multi objects separation within one chip of the respective pseudo-random noise (PRN) code. To deal with the problem, the first author's previous works [22], [23] proposed to use intermediate frequency (IF) GNSS signal for performing range compression and apply second order differentiation (Diff2) operator to range compressed pulses in 2017 and 2019, respectively. The results show that on the basis of GPS C/A code signal, range resolution can be enhanced to 40 m level from 150 m level. Moreover, [23] outer-performs [22], as the method in [23] will not degrade image signal-to-noise (SNR) level. At the same time, the literature [24] improves the algorithm in [23] by reducing side-lobe magnitude for range profiles.

To authors best knowledge, the performance of the new-generation GNSS signal, namely the Beidou B3I signal, remains unknown in the SAR imaging community. As the global construction of this system was completed in June 2020, few related studies had been conducted at the time of this writing. To date, the best range resolution reported in the GNSS-SAR-related literature only reached the meter level, indicating considerable room for improvement in terms of remote sensing applications for high-resolution imaging. Moreover, although single Diff2 operator [23], [24] can greatly enhance range resolution without distorting SNR with respect to numbers of sampling points (determined by sampling frequency), its impact is not unlimited. Through a respective investigation based on the methods in [23], [24], when sampling frequency reaches a certain level, the value of range resolution will not increase any more. For instance, in GPS C/A code signal based SAR, when sampling frequency increases to the level no less than 1.6×10^7 Hz, the range resolution value using the methods in [23] and [24] remains at 40 m. In summary, an evaluation of the performance of Beidou B3I SAR imaging and attempts to further improve the range resolution are strongly warranted, and will increase the applicability of this novel technique for environmental surveillance.

This paper firstly provides proof-of-concept verifications with respect to SAR imaging using Beidou B3I signal. To further improve the range resolution beyond the current best result via multipath signal separation, cascaded Diff2 operator and cascaded Teager-kaiser (TK) operator are proposed and applied to range compressed pulses, respectively. Thereafter, to eliminate the apparent side-lobes when performing multi-path signal separation and preserve original carrier phase value for the pulse at respective range domain, zero thresholding scheme and phase recovery processing are applied. Both simulation and the experiment with field Beidou B3I signal raw data were carried out to evaluate the proposed methods. The results show that indeed the main-lobe width of each range compressed pulse can be achieved at 0.4 m. This indicates that decimetre level range resolution can be obtained by the proposed methods, compared to 15 m based on conventional GNSS-SAR imaging method. Meanwhile, the achieved range resolution is significantly higher than current best result 3 m in GNSS-SAR related literatures [20]. Furthermore, according to the experimental results, the proposed method based on the cascaded TK operator outperforms that based on the cascaded Diff2 operator because the former causes less background interference.

The rest of the paper is organized as follows: The proposed imaging methods on the basis of both cascaded Diff2 operator and cascaded TK operator are given and analyzed in section II. The simulation and experiment with field Beidou B3I signal raw data are illustrated in section III and section IV, respectively. Section V discussed the associated issues and presents the respective future research direction. Section VI concludes the whole paper.

II. THE PROPOSED IMAGING METHODS OF DECIMETRE LEVEL RANGE RESOLUTION

The overall schematic diagram is shown in Figure 1.

In Figure 1, to separate direct and reflected B3I signals on passive SAR image, at the antenna module, two antennas i.e. direct antenna and surveillance antenna are employed for the respective signal collections, in which, direct B3I signal is for synchronization and reflected B3I signal is for remote sensing imaging of surveillance region. Meanwhile, to maximally avoid direct interference at surveillance channel, we considered the satellite in the backscattering geometric mode. At the receiver, the received B3I signals are down-converted into baseband, digitized and formatted into range and azimuth domains. To meet the goal of this paper decimetre range resolution, first of all, the distance between two sampling points at range domain should reach the decimetre level (less than 1 m). Denoting c as signal transmission speed, T_{code} as

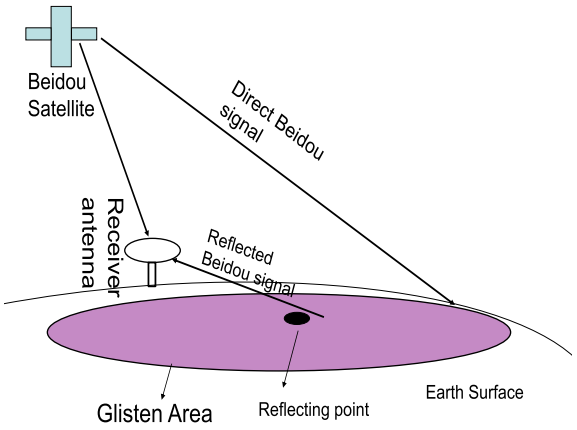

FIGURE 1. The overall schematic diagram.

code period, N_s as quantity of sampling points in each range domain, the following criterion should be satisfied:

$$\frac{c \cdot T_{code}}{N_s} < 1\ \text{m} \Rightarrow N_s > c \cdot T_{code}. \tag{1}$$

Normally $c = 3 \times 10^8$ m/s, $T_{code} = 1$ ms. Therefore on the basis of (1), N_s should no less than 3×10^5. The received direct signal at receiver for each satellite can be expressed as

$$S^i_{B3I\_D}(t,u) = A^D_{B3I} C^i_{B3I}(t,u) D^i_{B3I}(t) \cdot \exp\left(j\left(2\pi f_D t + \phi^i_D(u)\right)\right) + n_D(t,u) \tag{2}$$

where i represents index of satellite, A^D_{B3I} represents magnitude of direct B3I signal, C^i_{B3I} represents the pseudo-random noise (PRN) code of the i-th satellite, D^i_{B3I} represents the navigation bit of i-th satellite, f_D represents Doppler frequency, ϕ^i_D represents carrier phase of direct signal and n_D represents the background noise at direct channel.

The reflected B3I signal, which is a delayed version of direct signal, can be expressed as

$$S^i_{B3I\_R}(t-\tau,u) = \begin{cases} A^R_{B3I} C^i_{B3I}(t-\tau,u) D^i_{B3I}(t) \\ \exp\left(j\left(2\pi f_R t + \phi^i_R(u)\right)\right) & \text{precence of} \\ \quad + n_R(t,u), & \text{reflected signal} \\ n_R(t,u), & \text{absence of} \\ & \text{reflected signal} \end{cases} \tag{3}$$

where A^R_{B3I} represents magnitude of reflected B3I signal, τ represents the delay of reflected B3I signal compared to the respective direct signal, f_R represents Doppler frequency of reflected B3I signal, ϕ^i_R represents carrier phase of reflected B3I signal and n_R represents background noise at the surveillance channel. Since in this paper, both direct and surveillance antennas are installed on the same platform, we can have that $f_D = f_R$.

Synchronization on the basis of (2) is carried out [8]. The synchronized result is served as matched filter signal for range compression, which can be expressed as

$$S^i_{B3I\_M}(t,u) = C^i_{B3I}(t,u) D^i_{B3I}(t) \exp\left(j\left(2\pi f_D t + \phi^i_D(u)\right)\right). \tag{4}$$

Next, the imaging procedure is carried out. The conventional imaging method is well documented in [8], thus the respective analysis is omitted in this paper. For the proposed imaging methods, the first step is similar as conventional method, which is to perform correlation operation between (3) and (4). The respective expression can be seen as follows:

$$R(t-\tau,u) = S^i_{B3I\_R}(t-\tau,u) * \left(S^i_{B3I\_M}(t,u)\right)^* = \begin{cases} A^R_{B3I} \cdot \Lambda(t-\tau) \cdot D^i_{B3I}(t) \\ \cdot \exp\left(j\left(\phi^i_R(u) - \phi^i_D(u)\right)\right) & \text{Presence of} \\ \quad + n_R \cdot S^i_{B3I\_M}, & \text{reflected signal} \\ n_R \cdot S^i_{B3I\_M}, & \text{Absence of} \\ & \text{reflected signal} \end{cases} \tag{5}$$

where Λ represents the correlation function of pseudo-random noise (PRN) code of B3I signal.

Denoting $R_s(t-\tau,u) = A^R_{B3I} \cdot \Lambda(t-\tau) \cdot D^i_{B3I}(t) \cdot \exp\left(j\left(\phi^i_R(u) - \phi^i_D(u)\right)\right)$, on the basis of (5), the cascaded Diff2 operator and cascaded TK operator are performed. The procedure can be seen as follows.

Different from our previous work [23] and the work in [24], in order to avoid the unnecessary computations in the regions without reflected signals, the range domains which have the obvious correlated pulses are detected and selected for further processing. The respective rule for threshold setting can be expressed as follows:

$$T = \max\{R(t-\tau,u)\} \cdot w + n_R \cdot S^i_{B3I\_M} \tag{6}$$

where T represents the threshold and w represents the weighting factor. According to the criterion for detecting matched filtered signals [25], since Beidou B3I signal is binary phase shift keying (BPSK) modulated signal, the value w can be chosen within the interval [0.1, 0.5].

Thereafter the steps based on cascaded Diff2 and cascaded TK operators are performed, respectively. The original usage of Diff2 operator and TK operator can be seen in [25] for separating muti-path signals within one chip of PRN code based on code correlated pulse during direct signal tracking procedure. Since in Beidou B3I-SAR, multiple reflected signals can be regarded as multi-path signal, range compression can be approached as code correlation and the main-lobe width of range compressed pulse is the same as code correlated pulse width, in this remit, Diff2 operator (which has already been proved in [23] and [24]) and TK operator (in theoretical) can also be used for distinguishing multi reflections within one chip of PRN code, in which,

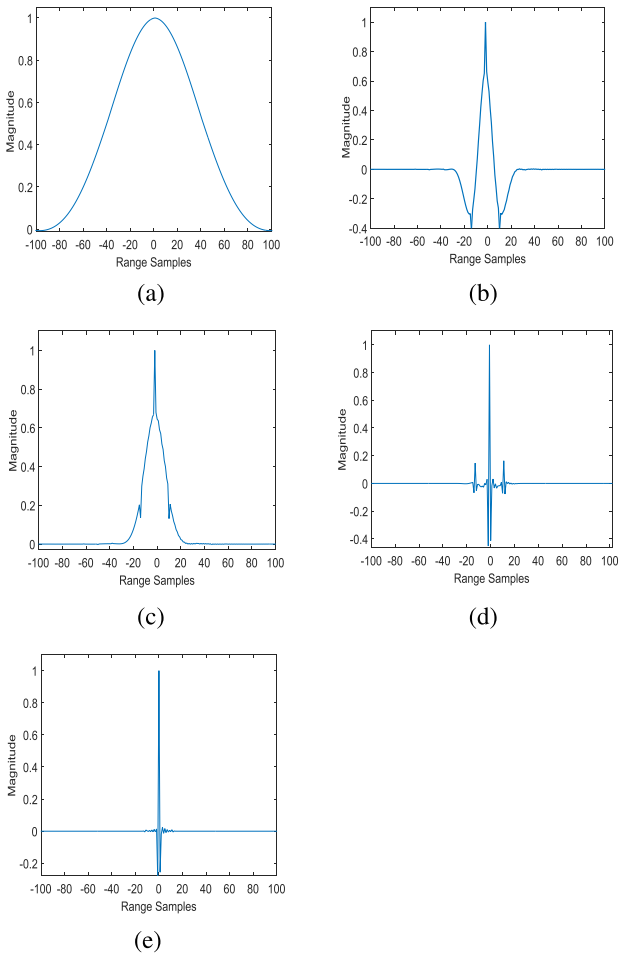

FIGURE 2. The range compressed pulses: (a) Conventional imaging method, (b) The method with single Diff2 operator at range domain, (c) The method with single TK operator at range domain, (d) The proposed method with cascaded Diff2 operator at range domain, (e) The proposed method with cascaded TK operator at range domain.

range resolution would be improved. However an initial test in this B3I signal-based research suggests that the single Diff2 operator or single TK operator can only improve the range resolution to the meter level. To achieve the goal decimetre range resolution in this paper, cascaded Diff2 operator or cascaded TK operator is performed on (5) under the rule (6) to further separate multiple aliased signals within the respective main-lobe region. Due to the fact that the related property is hard to be derived mathematically, to be intuitive for analysis, the preliminary simulation with respect to the normalized range compressed pulses for B3I-SAR signal processed by Diff2, TK, cascaded Diff2, cascaded TK operators with numbers of sampling points 1500000 (which satisfied the criterion in (1)) at each range domain are given in Figure 2.

From Figure 2, it can be seen that using cascaded Diff2 or cascaded TK operator, the main-lobe width of range compressed pulse has been greatly reduced. The respective detailed steps with respect to cascaded Diff2 and TK operator are introduced and analyzed as follows:

1). At first, perform first order Diff2 operator or TK operator. The respective performed first order Diff2 operator can be expressed as equation (7), as shown at the bottom of the next page, while the respective performed first order TK operator can be expressed as equation (8), as shown at the bottom of the next page. By performing (7) or (8), according to Figure 2(b) and (c), the main-lobe of (5) is narrowed with the width 10 samples. As the pulses are extracted from the range domain with numbers of sampling points 1500000, the main-lobe width in distance unit for Fig. 2(b) and (c) can be calculated as $\frac{3\times10^8 \text{ m/s}\times 1 \text{ ms}}{1500000} \times 10 = 2$ m, which indicates that meters level range resolution is achieved at first.

2). According to Figure 2(b), it can be seen that after performing the multi signal separation with Diff2 operator, normally there will bring two obvious symmetrical side-lobes beside main-lobe, which will interfere imaging result. However, thanks to the values of side-lobes are less than zero, thus, the zero thresholding method can be employed on (7) to eliminate the brought side-lobes. The respective expression can be seen as:

$$R^T_{diff\,2}(t-\tau, u) = \begin{cases} R_{diff\,2}(t-\tau, u), & \text{when } R_{diff\,2} \geq 0 \\ 0, & \text{when } R_{diff\,2} \leq 0 \end{cases} \tag{9}$$

where $R^T_{diff\,2}$ is the zero thresholded signal of (7).

3). To further improve range resolution to decimetre level, on the basis of (9), (8), cascaded Diff2 and TK operators are performed as equations (10) and (11), as shown at the bottom of the next page for further separating multi reflected signals within the main-lobe regions of the pulses in (9) and (8) respectively, where $R_{diff\,2\_cascaded}$ and $R_{TK\_cascaded}$ denotes cascaded Diff2 and TK operators. The results in this step corresponds to the preliminary simulation in Figure 2(d) (for cascaded Diff2 operator) and Figure 2(e) (for cascaded TK operator). It can be seen that the main-lobe width is further reduced to 2 sampling points, when transform into distance unit, we can have that $\frac{3\times10^8 \text{ m/s}\times 1 \text{ ms}}{1500000} \times 2 = 0.4$ m, which represents decimetre range resolution.

4). After performing 3), on the basis of Figure 2(d) and (e), the symmetrical side-lobes with the values less than zero appears again. To eliminate the side-lobes, zero thresholding scheme is applied again on (10) and (11), respectively.

After performing the steps above, the carrier phase component of the illuminated regions has been changed. From deviation, we can have that the carrier phase component is changed to $\exp\left(j4\left(\phi^i_R - \phi^i_D\right)\right)$. However, the original carrier phase component will be required for azimuth compression stage. In this remit, similar to [23] and [24], carrier phase recovery operator is generated, which steps can be seen as follows:

1). On the basis of (10) and (11), taking cascaded Diff2 operator as an example, generating 'Imag-Real Ratio' as equation (12), as shown at the bottom of the next page. Then, we can have that the original carrier phase difference between reflected and direct Beidou B3I signal can be mathematically expressed as equation (13), as shown at the bottom of the next page. For cascaded TK operator, in (11), denoting the term when $u \in \max\{R(t-\tau,u)\} \geq T$ as $R'_{TK\_cascaded}(t-\tau,u)$, similarly, we can have the respective original carrier phase difference between reflected and direct B3I signal as equation (14), as shown at the bottom of the next page;

2). On the basis of (13) and (14), generating phase recovery operators. For cascaded Diff2 method, the respective operator for illuminated region is generated as (15), as shown at the bottom of the next page; for cascaded TK method, the respective phase recovery operator is generated as follows

$$\exp\left(-j\frac{3}{4}\arctan\left(\frac{\mathrm{Imag}\left(R'_{TK\_cascaded}(t-\tau,u)\right)}{\mathrm{Real}\left(R'_{TK\_cascaded}(t-\tau,u)\right)}\right)\right), \quad \text{when } u \in \max\{R(t-\tau,u)\} \geq T \tag{16}$$

3). Multiplying (10) with (15), (11) with (16), phase recoveries procedure is completed.

Thereafter, on the basis of phase recovered results, azimuth compression is performed within the receiver's positions that contains illuminated regions.

Overall, the steps of the proposed methods are summarized in Algorithm 1.

III. THE PROOF OF CONCEPT SIMULATION EXPERIMENT

To test the feasibility with respect to the proposed imaging method for improving range resolution to decimetre level, a proof of concept simulation experiment is carried out. The respective parameter values are given in Table 1.

Based on Table 1, we can have that the distance between two range samples is

$$D = 3 \times 10^8 \mathrm{m/s} \times \frac{1\mathrm{ms}}{1500000} = 0.2\mathrm{m} \tag{17}$$

which provides a presupposition for decimetre range resolution achievement. Firstly the point spread function (PSF) with respect to conventional method and the proposed method on the basis of cascaded Diff2 operator and TK operator are simulated. The coordinate is transformed from samples to distance based on (17). The respective results are shown

$$R_{Diff2}(t-\tau,u) = \begin{cases} \left(R_s(t-\tau,u) + n_R \cdot S^i_{B3I\_M}\right) \\ \cdot\left(\dfrac{\partial^2}{\partial\tau^2}\left(R_s(t-\tau,u) + n_R \cdot S^i_{B3I\_M}\right)\right), & \text{when } u \in \max\{R(t-\tau,u)\} \geq T \\ n_R \cdot S^i_{B3I\_M}, & \text{when } u \in \max\{R(t-\tau,u)\} < T \end{cases} \tag{7}$$

$$R_{TK}(t-\tau,u) = \begin{cases} \left(R_s(t-\tau-1,u) + n_R \cdot S^i_{B3I\_M}\right) \cdot \left(R_s(t-\tau-1,u) + n_R \cdot S^i_{B3I\_M}\right)^* \\ -\dfrac{1}{2}\left\{\left(R_s(t-\tau-1,u) + n_R \cdot S^i_{B3I\_M}\right) \cdot \left(R_s(t-\tau,u) + n_R \cdot S^i_{B3I\_M}\right)^* \right. \\ \left. + \left(R_s(t-\tau,u) + n_R \cdot S^i_{B3I\_M}\right) \cdot \left(R_s(t-\tau-2,u) + n_R \cdot S^i_{B3I\_M}\right)^*\right\} \\ \qquad\qquad \text{when } u \in \max\{R(t-\tau,u)\} \geq T \\ n_R \cdot S^i_{B3I\_M}, \\ \qquad\qquad \text{when } u \in \max\{R(t-\tau,u)\} < T \end{cases} \tag{8}$$

$$R_{diff2\_cascaded}(t-\tau,u) = \begin{cases} R^T_{diff2}(t-\tau,u) \\ \cdot\dfrac{\partial^2}{\partial\tau^2}\left(R^T_{diff2}(t-\tau,u)\right), & \text{when } u \in \max\{R(t-\tau,u)\} \geq T \\ n_R \cdot S^i_{B3I\_M}, & \text{when } u \in \max\{R(t-\tau,u)\} < T \end{cases} \tag{10}$$

$$R_{TK\_cascaded}(t-\tau,u) = \begin{cases} R_{TK}(t-\tau-1,u) \cdot (R_{TK}(t-\tau-1,u))^* \\ -\dfrac{1}{2}\left\{R_{TK}(t-\tau-1,u) \cdot (R_{TK}(t-\tau,u))^* \right. & \text{when } u \in \max\{R(t-\tau,u)\} \\ \left. + R_{TK}(t-\tau,u) \cdot (R_{TK}(t-\tau-2,u))^*\right\}, & \geq T \\ n_R \cdot S^i_{B3I\_M}, & \text{when } u \in \max\{R(t-\tau,u)\} \\ & < T \end{cases} \tag{11}$$

TABLE 1. The parameter values for simulation experiment.

Parameters	Types or Values
Signal type	Beidou B3I signal
Operating frequency	1268.52 MHz (L1 band)
Distance between satellite orbit and earth surface	21528 km
Signal transmission velocity c	3×10^8 m/s
Code period T	1 ms
Signal bandwidth B	10.23 MHz
Sampling frequency	1.5×10^9 Hz
Number of samples at range domain N_s	1500000
Antenna gain + RF gain	20 dB
Boltzmann constant k	1.38×10^{-23} J/K
Experimental temperature	300 K

in Figure 3, in which, the illustrated range distance is cut within the interval [−6.4 m, 6.4 m].

From Figure 3, it can be seen that based on the proposed method, the main-lobe width of the PSF at range domain indeed greatly reduced to the level less than 1.6 m, compared to conventional imaging method. Meanwhile, compare Figure 3(b) to (c), it can bee seen that the raised background interference is much less for the proposed imaging method based on TK operator. To further evaluate main-lobe width at range domain for Figure 3(b) and (c), we zoomed the respective illuminated regions with the range distance interval [−1.2 m, 1.2 m] and azimuth distance interval [30°, 30°], which can be seen in Figure 4.

Based on Figure 4, it can be seen that the main-lobe width with respect to the proposed imaging method decreased to 0.4 m level. This indicates that the main-lobe width of auto-correlated B3I signal can be reduced to decimetres level.

Thereafter a simulation experiment with respect to reflected Beidou-B3I signal environment is carried out on the basis of the parameter values in Table 1. The simulation environment is shown in Figure 5.

In Figure 5, the simulated circular movement of the receiver is employed for synthetic aperture forming with a velocity $1^\circ/s$ and the duration 100 s. Thus the length of circular trace for forming synthetic aperture is 100°. As the trace is circular, the azimuth compression method in [26] is applied in imaging processing, which is different from traditional

$$
\begin{aligned}
&\delta_{diff2\_cascaded}\left(t-\tau,u\right)\\
&=\begin{cases}\dfrac{\mathrm{Imag}\left(R^T_{diff2}\left(t-\tau,u\right)\frac{\partial^2}{\partial\tau^2}R^T_{diff2}\left(t-\tau,u\right)\right)}{\mathrm{Real}\left(R^T_{diff2}\left(t-\tau,u\right)\frac{\partial^2}{\partial\tau^2}R^T_{diff2}\left(t-\tau,u\right)\right)}, & \text{when } u\in \max\left\{R\left(t-\tau,u\right)\right\}\geq T\\ n_R\cdot S^i_{B3I\_M}, & \text{when } u\in \max\left\{R\left(t-\tau,u\right)\right\}<T\end{cases}\\
&=\begin{cases}\dfrac{\sin\left(4\left(\phi^i_R\left(u\right)-\phi^i_D\left(u\right)\right)\right)}{\cos\left(4\left(\phi^i_R\left(u\right)-\phi^i_D\left(u\right)\right)\right)}, & \text{when } u\in \max\left\{R\left(t-\tau,u\right)\right\}\geq T\\ n_R\cdot S^i_{B3I\_M}, & \text{when } u\in \max\left\{R\left(t-\tau,u\right)\right\}<T\end{cases}\\
&=\begin{cases}\tan\left(4\left(\phi^i_R\left(u\right)-\phi^i_D\left(u\right)\right)\right), & \text{when } u\in \max\left\{R\left(t-\tau,u\right)\right\}\geq T\\ n_R\cdot S^i_{B3I\_M}, & \text{when } u\in \max\left\{R\left(t-\tau,u\right)\right\}<T\end{cases}
\end{aligned}
\tag{12}
$$

$$
\phi^i_R\left(u\right)-\phi^i_D\left(u\right)=\begin{cases}\dfrac{1}{4}\arctan\left(\dfrac{\mathrm{Imag}\left(R^T_{diff2}\left(t-\tau,u\right)\frac{\partial^2}{\partial\tau^2}R^T_{diff2}\left(t-\tau,u\right)\right)}{\mathrm{Real}\left(R^T_{diff2}\left(t-\tau,u\right)\frac{\partial^2}{\partial\tau^2}R^T_{diff2}\left(t-\tau,u\right)\right)}\right), & \text{when } u\in \max\left\{R\left(t-\tau,u\right)\right\}\geq T\\ n_R\cdot S^i_{B3I\_M}, & \text{when } u\in \max\left\{R\left(t-\tau,u\right)\right\}<T\end{cases}
\tag{13}
$$

$$
\phi^i_R\left(u\right)-\phi^i_D\left(u\right)=\begin{cases}\dfrac{1}{4}\arctan\left(\dfrac{\mathrm{Imag}\left(R'_{TK\_cascaded}\left(t-\tau,u\right)\right)}{\mathrm{Real}\left(R'_{TK\_cascaded}\left(t-\tau,u\right)\right)}\right), & \text{when } u\in \max\left\{R\left(t-\tau,u\right)\right\}\geq T\\ n_R\cdot S^i_{B3I\_M}, & \text{when } u\in \max\left\{R\left(t-\tau,u\right)\right\}<T\end{cases}
\tag{14}
$$

$$
\exp\left(-j\frac{3}{4}\arctan\left(\frac{\mathrm{Imag}\left(R^T_{diff2}\left(t-\tau,u\right)\frac{\partial^2}{\partial\tau^2}R^T_{diff2}\left(t-\tau,u\right)\right)}{\mathrm{Real}\left(R^T_{diff2}\left(t-\tau,u\right)\frac{\partial^2}{\partial\tau^2}R^T_{diff2}\left(t-\tau,u\right)\right)}\right)\right),\quad \text{when } u\in \max\left\{R\left(t-\tau,u\right)\right\}\geq T
\tag{15}
$$

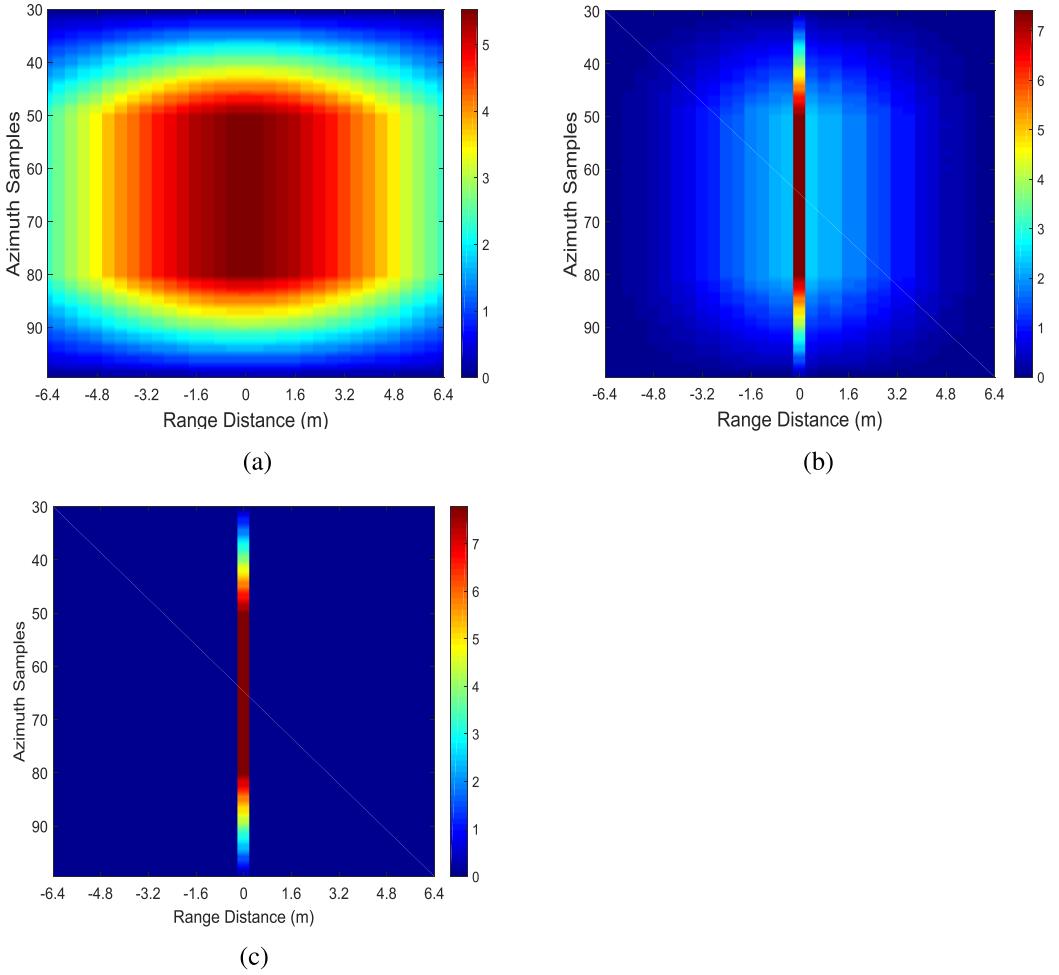

FIGURE 3. The PSF of Beidou-B3I SAR: (a) Conventional imaging method, (b) The proposed method with cascaded Diff2 operator at range domain, (c) The proposed method with cascaded TK operator at range domain.

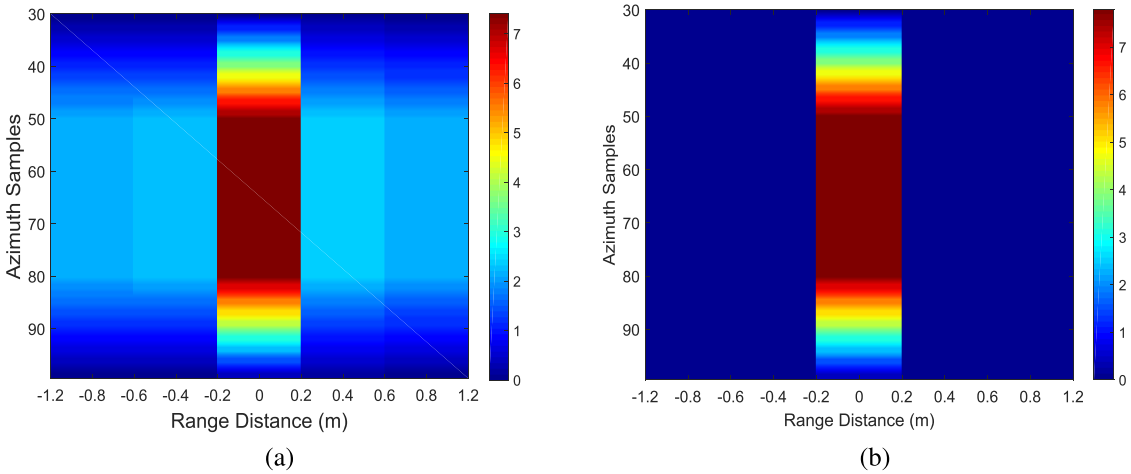

FIGURE 4. The zoomed PSF of Beidou-B3I SAR: (a) The proposed imaging method with cascaded Diff2 operator at range domain, (b) The proposed method with cascaded TK operator at range domain.

straight trace of coherent integration over slow-time domain. Since azimuth compression method is not concentrated in this paper, the respective descriptions are omitted. On the ground, it is assumed that there exists three strong reflecting regions. For the ease of examining, the receiver and the strong scattered objects are simulated in the same horizontal axis,

Algorithm 1 The Work-Flow of the Proposed Method Based on Cascaded Diff2 or Cascaded TK Operators

1. On the basis of output of signal synchronized results, selecting the satellite that satisfied the geometric position as Figure 1;
2. Generating the respective local replica as matched filter signal for range compression as (4);
3. Performing correlation operation between reflected and direct B3I signals as (5);
4. Selecting the range periods which have obvious compressed pulses in step 3 on the basis of (6) for the lateral processing;
5. Performing cascaded Diff2 operator or cascaded TK operator as (10) or (11);
6. Generating phase recovery operators as (15) and (16) for cascaded Diff2 operator and cascaded TK operator, respectively;
7. Applying the phase recovery operators in (15) and (16) to (10) and (11), respectively;
8. Performing azimuth compression based on the results in step 7;
9. On the basis of the result in step 8, performing the absolute operator;
10. Obtaining range resolution improved Beidou B3I-SAR image.

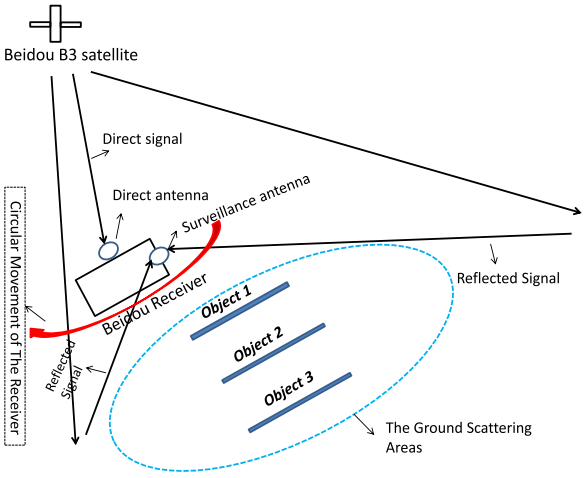

FIGURE 5. The simulation environment.

which can be considered as a quasi-monostatic model. The range distance between each region is 7 m. The size of each region is 0.2 m at range domain and 30° circular distance at azimuth domain. The background noise is assumed to be additive white Gaussian noise (AWGN). The simulated Beidou-B3I SAR images with respect to conventional imaging method and the proposed methods on the basis of both cascaded Diff2 operator and cascaded TK operator are illustrated in Figure 6.

As shown in Figure 6(a), when using the conventional imaging method, the range resolution can only be obtained at the level of 15 m because the B3I signal bandwidth is restricted at a value of 10.23 MHz. Therefore, it is hard to separate three strong reflecting regions at range domain. From Figure 6(b) and (c), because the proposed methods based on cascaded Diff2 and TK operators can largely reduce the main-lobe ambiguity of range compressed signal to decimetre level, the three scattering regions can be easily distinguished. Moreover the object-background contrast in Figure 6(c) is higher than (b). All these results in Figure 6 indicate that under simulated remote sensing imaging environment, decimetre level range resolution can be obtained, and the caused background interference level with cascaded TK operator is much less than cascaded Diff2 operator.

IV. THE PROOF OF CONCEPT EXPERIMENT WITH FIELD DATA CONFIRMATION

To further demonstrate the feasibility of the proposed imaging methods, a proof of concept experiment with field Beidou-B3I signal data was carried out at the roof garden of the engineering building, Changsha University. The experimental scenario is given in Figure 7.

In this experiment, the objects are two reflection boards, which face to the west and the distances to Beidou B3I receiver are 7 m. Both direct antenna and surveillance antenna are employed for collecting direct B3I signals from satellites and reflected B3I signals from surveillance area simultaneously, respectively, in which, direct antenna is right-handed elliptically polarised and faces to the sky, while surveillance antenna is left-handed elliptically polarised and faces to the two reflecting boards. The movement of rotation shaft is used for performing circular trace of surveillance antenna. The speed of rotation shaft is 1.67°/s with the duration 60 s. Because the trace is circular, similar as section III, the azimuth compression method in [26] is used for forming synthetic aperture. The collected raw Beidou-B3I signal data are down converted to baseband and digitized at the respective software defined radio (SDR) receiver front end (produced by Beijing CNSENS Technology Company), formatted into range and azimuth domain and then saved into laptop computer. The imaging procedure were accomplished on computer platform using the software MATLAB 2015a.

The parameter values in this section is the same as Table 1. The positions of each Beidou satellites during the experiment are provided in Figure 8, which was extracted from GNSS View software.

Based on Figure 8, the satellite Beidou C27 is selected as transmitter of opportunity, as it satisfies backscattering geometric mode as Figure 1 for maximally avoiding direct signal interference at surveillance antenna, also, the respective signal quality is the best according to the synchronized results.

Based on the experimental scenario and the signal from the satellite C27, the imaging results with respect to conventional method and the proposed method using cascaded Diff2 and cascaded TK operators are shown in Figure 9.

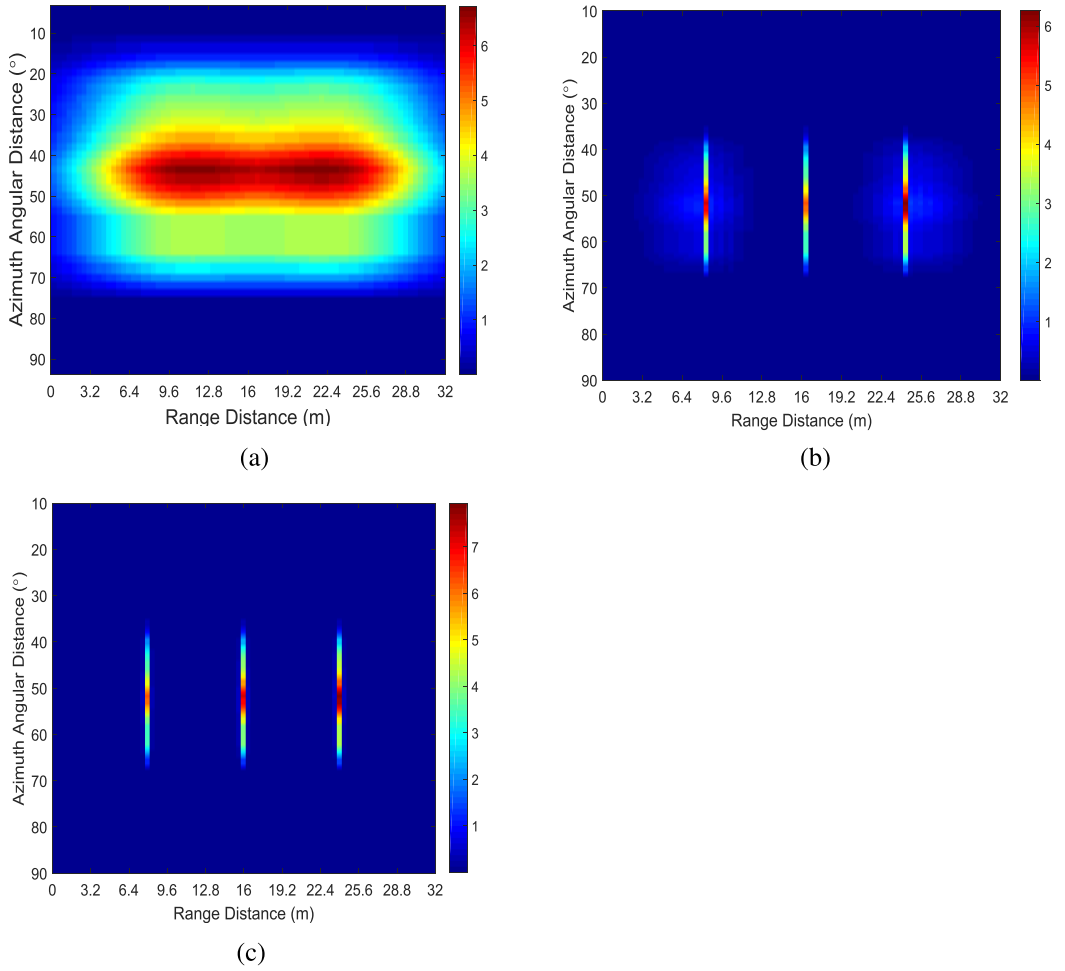

FIGURE 6. The simulated of Beidou-B3I SAR images: (a) Conventional imaging method, (b) The proposed method with cascaded Diff2 operator at range domain, (c) The proposed method with cascaded TK operator at range domain.

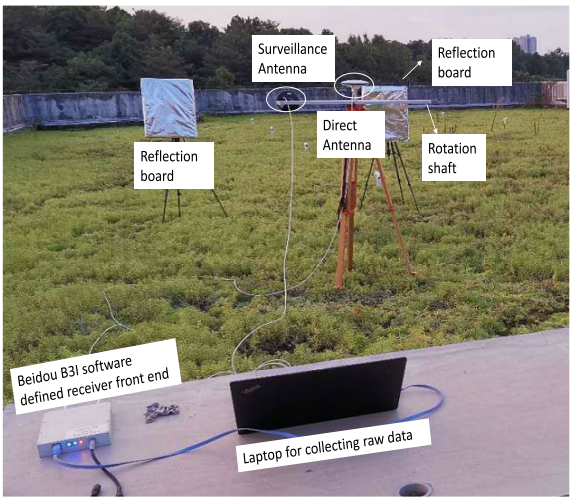

FIGURE 7. The field experimental scenario.

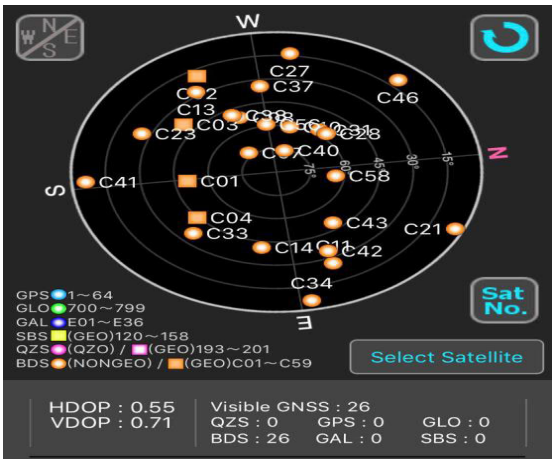

FIGURE 8. The Beidou satellites positions during the experiment.

For comparison, the range axis of all sub figures in Figure 9 are chosen within the interval $[-22.5\text{m}, 37.5\text{m}]$, while the azimuth axis are chosen within the interval $[0°, 100°]$.

In Figure 9, similar as the simulation, indeed the main lobe width at range domain of the illuminated areas are much less for the proposed imaging methods, compared to conventional imaging method. This reveals that range resolution is

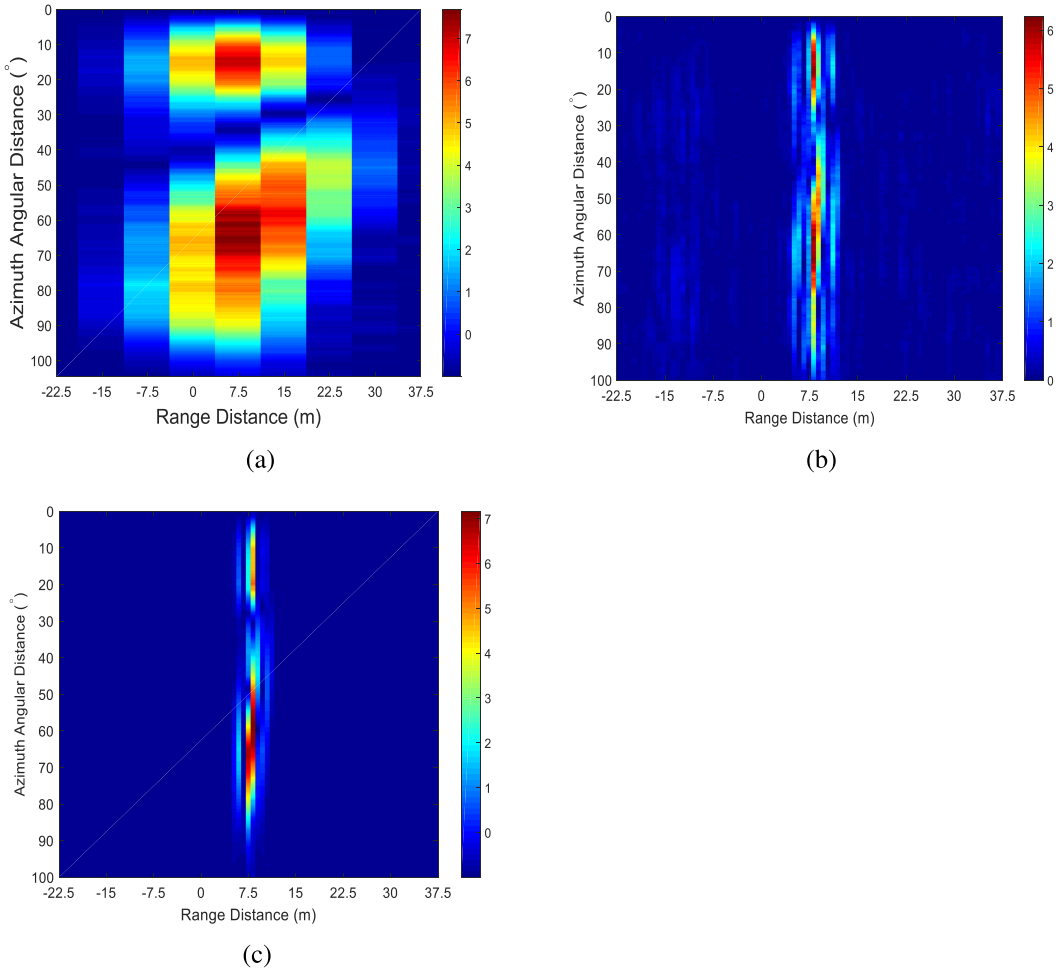

FIGURE 9. The Beidou-B3I SAR images using field data: (a) Conventional imaging method, (b) The proposed method with cascaded Diff2 operator at range domain, (c) The proposed method with cascaded TK operator at range domain.

significantly improved. Compare Figure 9(c) to (b), it can be seen that the same as the simulation results, background interference after resolution enhancement is indeed less for cascaded TK operator. The other less illuminated region in Figure 9(c) may come from the surroundings such as grass. For a better examining the obtained range resolution level based on the proposed method, we zoomed one of the illuminated regions in both Figure 9(b) and (c). The respective result are shown in Figure 10.

Based on Figure 10, through the measurement using MATLAB, it can be seen that indeed the main-lobe width at range domain of the illuminated region has been reduced to 0.4 m level. This indicates that the range resolution can be achieved at decimetre level on the basis of field Beidou-B3I signal as well. Furthermore, we can have the same verdict as section III that between the proposed imaging methods, cascaded TK operator outer-performs cascaded Diff2 operator, as its background interference level is less.

V. DISCUSSION

This paper provides a proof-of-concept demonstration of the achievement of Beidou-B3I SAR imaging at a decimeter-range resolution. However, the following issues require further consideration.

- In the experimental demonstration, the range compression method based on the cascaded TK operator outperformed that based on the cascaded Diff2 operator because the former caused less background interference. However, as the main goal of this paper is to provide a preliminary proof-of-concept verification of the two proposed methods, more complicated field application scenarios such as ship or aircraft surveillance scenarios corresponding to the two methods have not been investigated in detail. This issue warrants investigation before implementing Beidou B3I-SAR in field environmental surveillance applications.
- In this work, both a simulation experiment and a field experiment with raw Beidou B3I signal data were performed using strong reflectors. The SNR was not the main focus. This is because we aimed only to provide a proof-of-concept experimental demonstration with respect to the achievement of a decimeter-level range resolution with the proposed imaging methods,

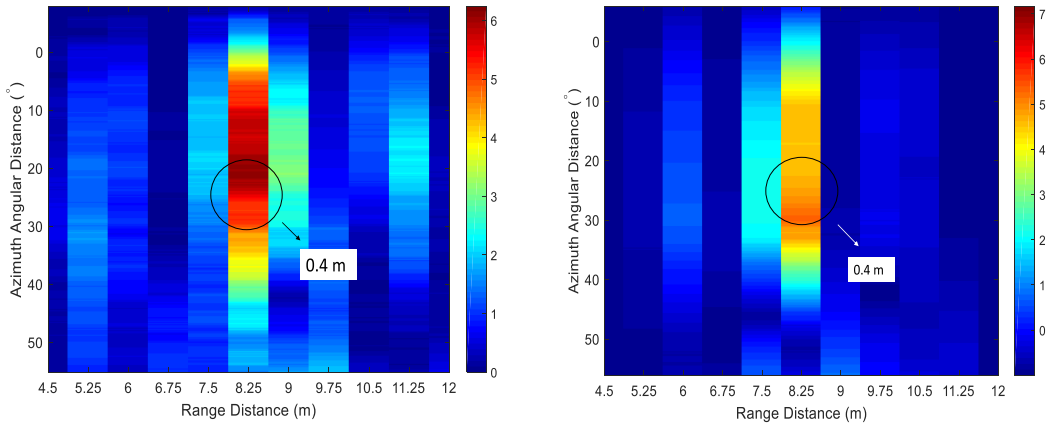

FIGURE 10. (a) The zoomed Beidou-B3I SAR images of Figure 9(b), (b) The zoomed Beidou-B3I SAR images of Figure 9(c).

the other distractions which may affect experimental results should be eliminated. However, the SNR is relatively low in many potential field environmental surveillance applications of Beidou B3I-SAR, and under such scenarios, the correlation peak of the range compressed pulse would not be very apparent. This issue will pose challenges to the achievement of range resolution enhancement at the decimeter level. Accordingly, the achievement of such high range resolutions under low SNR conditions remains to be explored.

Based on the two issues presented above, our future work will initially explore the difference between the two methods in detail under more complex environmental sensing scenarios, such as maritime object detection and aircraft imaging, to determine which method is more applicable. Secondly, we will study the ability of the imaging method to achieve decimeter-level range resolutions under low SNR circumstances. If the peak of range compressed pulses can be appeared after certain enhancement, theoretically the proposed methods can also be applied. Since our group has already obtained decent results with respect to imaging gain enhancement using coherently integrated multiple satellite signals [27], we are now working on the method that combining our previously proposed scheme [27] with the two methods proposed in this paper, to achieve the goal of decimetre level resolution for Beidou B3I-SAR imaging under low SNR conditions.

VI. CONCLUSION

This paper provides a proof-of-concept demonstration with respect to the achievement of a decimeter-level range resolution for GNSS-SAR imaging based on the Beidou B3I signal, a new-generation GNSS signal. Imaging methods based on the cascaded Diff2 and cascaded TK operators for range compression are proposed. To validate the proposed imaging methods, both a simulation experiment and a field experiment with raw B3I signal data are designed. According to the experimental results, the use of the proposed imaging method with either the cascaded Diff2 or cascaded TK operator for range compression can improve the range resolution to a level of 0.4 m, which is significantly higher than the current best result, 3 m, achieved with Galileo E5 signal based SAR. Furthermore, the use of the cascaded TK operator for range compression with the proposed method can reduce the background interference level to a greater extent than the cascaded Diff2 operator. This research should provide helpful insights and opportunities with respect to high-range resolution remote sensing imaging based on the Beidou B3I signal and can broaden the scope of application of the Beidou technique.

ACKNOWLEDGMENT

The authors would like to thank Prof. Wu Chen from the Hong Kong Polytechnic University for the software support of this article.

REFERENCES

[1] K. Borre, D. M. Akos, and N. Bertelsen, *A Software-Defined GPS and Galileo Receiver: A Single-Frequency Approach*. New York, NY, USA: Springer, 2007.

[2] E. Kaplan and C. Hegarty, *Understanding GPS: Principles and Applications*. Norwood, MA, USA: Artech House, 2005.

[3] Y. Yang, W. Gao, S. Guo, Y. Mao, and Y. Yang, "Introduction to BeiDou-3 navigation satellite system," *Navigation*, vol. 66, no. 1, pp. 7–18, 2019.

[4] R. Zuo, "Bistatic synthetic aperture radar using GNSS as transmitters of opportunity," Ph.D. dissertation, Dept. Electron., Elect., Comput. Eng., Univ. Birmingham, Birmingham, U.K., 2012.

[5] Z. Zeng, "Passive bistatic SAR with GNSS transmitter and a stationary receiver," Ph.D. dissertation, Dept. Electron., Elect., Comput. Eng., Univ. Birmingham, Birmingham, U.K., 2013.

[6] J. C. Curlander and R. N. McDonough, *Synthetic Aperture Radar*. New York, NY, USA: Wiley, 1991.

[7] M. A. Attalah, T. Laroussi, F. Gini, and M. S. Greco, "Range-Doppler fast block LMS algorithm for a DVB-T-based passive bistatic radar," *Signal, Image Video Process.*, vol. 13, no. 1, pp. 27–34, Feb. 2019.

[8] M. Antoniou and M. Cherniakov, "GNSS-based bistatic SAR: A signal processing view," *EURASIP J. Adv. Signal Process.*, vol. 2013, no. 1, pp. 1–16, Dec. 2013.

[9] H. Ma, M. Antoniou, D. Pastina, F. Santi, F. Pieralice, M. Bucciarelli, and M. Cherniakov, "Maritime moving target indication using passive GNSS-based bistatic radar," *IEEE Trans. Aerosp. Electron. Syst.*, vol. 54, no. 1, pp. 115–130, Feb. 2018.
[10] M. Antoniou, Z. Zeng, L. Feifeng, and M. Cherniakov, "Experimental demonstration of passive BSAR imaging using navigation satellites and a fixed receiver," *IEEE Geosci. Remote Sens. Lett.*, vol. 9, no. 3, pp. 477–481, May 2012.
[11] M. Antoniou, Z. Hong, Z. Zhangfan, R. Zuo, Q. Zhang, and M. Cherniakov, "Passive bistatic synthetic aperture radar imaging with Galileo transmitters and a moving receiver: Experimental demonstration," *IET Radar, Sonar Navigat.*, vol. 7, no. 9, pp. 985–993, Dec. 2013.
[12] F. Liu, M. Antoniou, Z. Zeng, and M. Cherniakov, "Point spread function analysis for BSAR with GNSS transmitters and long dwell times: Theory and experimental confirmation," *IEEE Geosci. Remote Sens. Lett.*, vol. 10, no. 4, pp. 781–785, Jul. 2013.
[13] F. Santi, D. Pastina, M. Bucciarelli, M. Antoniou, D. Tzagkas, and M. Cherniakov, "Passive multistatic SAR with GNSS transmitters: Preliminary experimental study," in *Proc. 11th Eur. Radar Conf.*, Oct. 2014, pp. 129–132.
[14] S. Shi, J. Liu, T. Li, and W. Tian, "Basic performance of space-surface bistatic SAR using BeiDou satellites as transmitters of opportunity," *GPS Solutions*, vol. 21, no. 2, pp. 727–737, Apr. 2017.
[15] F. Santi, D. Pastina, and M. Bucciarelli, "Maritime moving target detection technique for passive bistatic radar with GNSS transmitters," in *Proc. 18th Int. Radar Symp. (IRS)*, Jun. 2017, pp. 1–10.
[16] T. Zeng, T. Zhang, W. Tian, and C. Hu, "Space-surface bistatic SAR image enhancement based on repeat-pass coherent fusion with BeiDou-2/compass-2 as illuminators," *IEEE Geosci. Remote Sens. Lett.*, vol. 13, no. 12, pp. 1832–1836, Dec. 2016.
[17] H. Ma, M. Antoniou, A. G. Stove, J. Winkel, and M. Cherniakov, "Maritime moving target localization using passive GNSS-based multistatic radar," *IEEE Trans. Geosci. Remote Sens.*, vol. 56, no. 8, pp. 4808–4819, Aug. 2018.
[18] T. Zeng, D. Ao, C. Hu, T. Zhang, F. Liu, W. Tian, and K. Lin, "Multiangle BSAR imaging based on BeiDou-2 navigation satellite system: Experiments and preliminary results," *IEEE Trans. Geosci. Remote Sens.*, vol. 53, no. 10, pp. 5760–5773, Oct. 2015.
[19] F. Santi, M. Antoniou, and D. Pastina, "Point spread function analysis for GNSS-based multistatic SAR," *IEEE Geosci. Remote Sens. Lett.*, vol. 12, no. 2, pp. 304–308, Feb. 2015.
[20] H. Ma, M. Antoniou, and M. Cherniakov, "Passive GNSS-based SAR resolution improvement using joint Galileo E5 signals," *IEEE Geosci. Remote Sens. Lett.*, vol. 12, no. 8, pp. 1640–1644, Aug. 2015.
[21] F. Santi, M. Bucciarelli, D. Pastina, M. Antoniou, and M. Cherniakov, "Spatial resolution improvement in GNSS-based SAR using multistatic acquisitions and feature extraction," *IEEE Trans. Geosci. Remote Sens.*, vol. 54, no. 10, pp. 6217–6231, Oct. 2016.
[22] Y. Zheng, Y. Yang, and W. Chen, "A novel range compression algorithm for resolution enhancement in GNSS-SARs," *Sensors*, vol. 17, no. 7, p. 1496, Jun. 2017.
[23] Y. Zheng, Y. Yang, and W. Chen, "New imaging algorithm for range resolution improvement in passive global navigation satellite system-based synthetic aperture radar," *IET Radar, Sonar Navigat.*, vol. 13, no. 12, pp. 2166–2173, Dec. 2019.
[24] Y. Fang, J. Chen, P. Wang, and X. Zhou, "An image formation algorithm for bistatic SAR using GNSS signal with improved range resolution," *IEEE Access*, vol. 8, pp. 80333–80346, 2020.
[25] M. Z. H. Bhuiyan, E. S. Lohan, and M. Renfors, "Code tracking algorithms for mitigating multipath effects in fading channels for satellite-based positioning," *EURASIP J. Adv. Signal Process.*, vol. 2008, no. 1, Dec. 2007, Art. no. 863629.
[26] L. Chen, D. An, and X. Huang, "A backprojection-based imaging for circular synthetic aperture radar," *IEEE J. Sel. Topics Appl. Earth Observ. Remote Sens.*, vol. 10, no. 8, pp. 3547–3555, Aug. 2017.
[27] Y. Zheng, Z. Zhang, L. Feng, P. Zhu, and F. Zhou, "Enhanced passive GNSS-based radar imaging based on coherent integrated multi-satellite signals," *Sensors*, vol. 20, no. 3, p. 842, Feb. 2020.

YU ZHENG received the bachelor's degree in engineering from Xiangtan University, China, in June 2012, the M.Sc. degree from the University of Alberta, Canada, in November 2014, and the Ph.D. degree in philosophy from the Department of Land Surveying and Geo-Informatics, The Hong Kong Polytechnic University, in 2018. He is currently a Lecturer with the College of Electronic Communication and Electrical Engineering, Changsha University. His major research interests include environmental sensing using GNSS signals as source of opportunity and indoor location and surveillance using commercial devices.

He serves as a Reviewer for several international journals and conferences, such as *Sensors* and *Remote Sensing*.

ZHUXIAN ZHANG received the bachelor's degree from the Beijing University of Technology, China, in 2007, and the master's degree from The University of Melbourne, Australia, in 2009. She is currently pursuing the Ph.D. degree with the College of Electronic Science, National University of Defense Technology, China. After that, she joined the College of Electronic Communication and Electrical Engineering, Changsha University, China, as a Faculty Member. Her main research interests include high resolution imaging scheme using passive GNSS based radar and interference resistant mechanism for passive radar based on Compass (Beidou) signal.

PENG WU was born in 1983. He received the Ph.D. degree from the College of Electronic Science, National University of Defense Technology, Changsha, China. After that, he had been a Lecturer with the National University of Defense Technology. Since April 2019, he has been a Lecturer with the College of Electronic Communication and Electrical Engineering, Changsha University. His research interest includes signal processing for Beidou B2 and B3 systems. He serves as a Reviewer for many international journals, including IEEE Access and *GPS Solutions*.

PEIDONG ZHU (Senior Member, IEEE) received the Ph.D. degree in philosophy from the College of Computer Science and Technology, National University of Defense Technology, Changsha, China, in 1999.

After that, he has been a Faculty Member with the National University of Defense Technology, from a Lecturer to a Full Professor. He was a Visiting Chair Professor with Saint Xavier University, from 2008 to 2009. He is currently a Full Professor and the Departmental Header with the College of Electronic Communication and Electrical Engineering, Changsha University, Changsha. His main research interests include wireless communication networks and security assessment for radar networks. He published over 150 technical papers in different journals and conferences. He severed as a Reviewer for many technical journals, such as IEEE Transactions on Smart Grid and IEEE Access.